



## An improved model for hydromechanical coupling during shearing of rock joints

R. Olsson<sup>a,\*</sup>, N. Barton<sup>b</sup>

<sup>a</sup>Statkraft Grøner AS, P.O. Box 400, N-1327 Lysaker, Norway

<sup>b</sup>Nick Barton and Associates, Oslo, Norway and Sao Paulo, Brazil

Accepted 13 December 2000

### Abstract

This paper presents some experimental results from hydromechanical shear tests and an improved version of the original model suggested by Barton (Office of Nuclear Waste Isolation, Columbus, Ohio, ONWI-308, 1982, 96pp.) for the hydromechanical coupling of rock joints. The original model was developed for coupling between mechanical and hydraulic aperture change during normal loading and unloading. The method was also suggested for the coupling of shear dilation and hydraulic aperture changes. The improved model has the same appearance as the original and is based on hydromechanical shear experiments on granite rock joints. It includes both the mechanical and hydraulic aperture and the mobilised joint roughness coefficient ( $JRC_{mob}$ ). © 2001 Elsevier Science Ltd. All rights reserved.

### 1. Introduction

As a consequence of engineering works in a rock mass, deformation of both the joints and intact rock will usually occur as a result of the stress changes. Examples of such works are repositories for radioactive waste, dam foundations, excavation of tunnels and caverns, geothermal energy plants, oil and gas production, etc. Due to the stiffer rock matrix, most deformation occurs in the joints, in the form of normal and shear displacement. If the joints are rough, deformations will also change the joint aperture and fluid flow.

Traditionally, fluid flow through rock joints has been described by the cubic law, which follows the assumption that the joints consist of two smooth, parallel plates. Real rock joints, however, have rough walls and variable aperture, as well as asperity areas where the two opposing surfaces of the joint walls are in contact with each other.

According to this, apertures can generally be defined as *mechanical* (geometrically measured such as with epoxy injection) or *hydraulic* (measured by analysis of the fluid flow).

#### 1.1. Mechanical aperture ( $E$ )

The *mechanical* joint aperture ( $E$ ) is defined as the average point-to-point distance between two rock joint surfaces (see Fig. 1), perpendicular to a selected plane. If the joint surfaces are assumed to be parallel in the  $x$ - $y$  plane, then the aperture can be measured in the  $z$  direction. Often, a single, average value is used to define the aperture, but it is also possible to describe it stochastically. The aperture distribution of a joint is only valid at a certain state of rock stress and pore pressure. If the effective stress and/or the lateral position between the surfaces changes, as during shearing, the aperture distribution will also be changed.

Usually, the mechanical aperture is determined from a two-dimensional (2-D) joint section, which is a part compound of the real 3-D surface.

#### 1.2. Hydraulic aperture

The *hydraulic* aperture ( $e$ ) can be determined both from laboratory fluid-flow experiments [1–4], and bore-hole pump tests in the field [5,6].

Fluid flow through rock joints is often represented (assumed) as laminar flow between two parallel plates. The equivalent, smooth wall hydraulic aperture ( $e$ ) can

\*Corresponding author. Tel.: +47-6712-8000; fax: +47-6712-8212.

E-mail address: rol@statkraftgroner.no (R. Olsson).

<sup>1</sup>Formerly at Chalmers University of Technology, Gothenburg, Sweden.

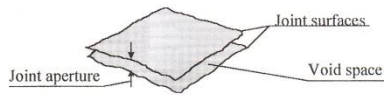


Fig. 1. Definition of mechanical joint aperture.

be obtained from flow tests using the modified form of Darcy's law relating flow rate ( $Q$ ) and gradient ( $dP/dy$ ):

$$Q = \frac{g}{v} \frac{w e^3}{12} \frac{dP}{dy}, \quad (1)$$

where  $w$  is the width of the flow path and  $v$  is the kinematic viscosity. This relation is also called the "cubic law". Here, only a single value is obtained for the aperture and the validity of Eq. (1) for natural rock joints, has been discussed by many authors.

An important distinction has to be made between the theoretical smooth wall hydraulic aperture ( $e$ ) and the real mechanical aperture ( $E$ ) (geometrically measured) between two irregular joint walls (Fig. 1). Owing to the wall friction and the tortuosity,  $E$  is generally larger than  $e$  during normal loading and unloading, which means that a rough joint requires a larger aperture than a smooth joint for the same water conducting capacity [7].

### 1.3. Fluid flow

The fluid flow in a rock mass is usually governed by three factors: the fluid properties, the void geometry and the fluid pressure at the joint boundary. The void geometry, i.e. the geometry of the volume between the joint surfaces, is governed by the geological history and can be described by several geometrical parameters, as aperture, frequency distribution, spatial correlation and contact area [8]. These geometrical parameters are related in various ways to the joint void geometry, as shown in Fig. 2.

Briefly, the properties can be described as follows:

- Aperture — the separation between the two joint wall surfaces.
- Roughness — the surface height distribution or the shape of the surfaces.
- Contact area — the area where the surfaces are in contact, and can transfer stresses.
- Matedness — how well matched the surfaces are.
- Spatial correlation — how abruptly or slowly the aperture changes from one point to another.
- Tortuosity — the forced bending of the stream lines due to variations in joint aperture.
- Channelling — differences in flow velocity along certain paths, due to variations in joint aperture.
- Stiffness — the stiffness or mechanical properties of a joint, which may be studied by looking at the closure caused by applied normal load.

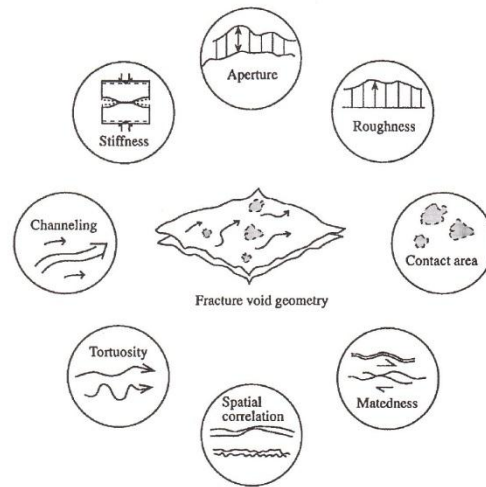


Fig. 2. Fracture (herein = joint) properties determined by fracture void geometry [8].

### 1.4. Hydromechanical coupling

In a rock mass, mechanical deformations will mainly occur as normal and/or shear deformations in the joints. This deformation will also change the joint aperture. By coupling the mechanical aperture changes to the hydraulic aperture changes, a hydromechanical coupling is achieved.

Most research concerning hydromechanical coupling in rock joints has been focused on the connection between normal loading and unloading and their effect on joint conductivity. The fact that shearing of rock joints can give an increasing or decrease of joint conductivity was highlighted during the International Symposium "Percolation through fissured rock" in 1972 [9–11].

Perhaps, one of the first flow experiments under concurrent shearing was performed on a cleavage plane in slate, and was reported by Sharp and Maini [10]. During the tests, no normal stress was applied, except for the dead weight; the joint was thus free to dilate. After a shear displacement of around 0.7 mm, the conductivity had increased by two orders of magnitude.

In the laboratory environment, hydromechanical shear experiments on joints with a normal stress higher than the dead weight were first reported by Makurat [12] at the Norwegian Geotechnical Institute (NGI). The test performed on a joint in gneiss with a constant water head of 2.8 m and with an effective normal stress of 0.82 MPa showed an increase of the permeability by two to three orders of magnitude after a shear displacement of around 1 mm. In the field, Hardin et al. [13] had

reported minor increases in conducting aperture when attempting to shear a diagonal joint in a  $2 \times 2 \times 2$  m block test in quartz monzonite gneiss. However, the joint concerned was very rough and the block was attached at its base.

A constitutive model relating the hydraulic aperture ( $e$ ) with the real mechanical aperture ( $E$ ) and the joint roughness (JRC) was proposed by Barton [14] and Barton, Bandis and Bakhtar [15]. The model was developed for coupling between mechanical and hydraulic aperture changes during normal loading and unloading and also for dilatant shearing of rock joints. Unfortunately, it seems that this is the only equation for hydromechanical coupling during shear of rock joints.

Based on new hydromechanical shear experiments on granite rock joints [16,17] an improved empirical model will be suggested for shearing, dilatant joints. It has the same appearance as the original and includes both the mechanical ( $E$ ) and hydraulic ( $e$ ) aperture. However, the mobilised Joint Roughness Coefficient (JRC<sub>mob</sub>) [14] is used in place of JRC<sub>peak</sub>.

## 2. Joint aperture — fluid flow and hydromechanical coupling

Fluid flow through a porous medium such as many soils and sedimentary rocks, can be described by Darcy's law (1-D flow):

$$Q = KiA, \quad (2)$$

where  $Q$  is the volumetric flow per unit area  $A$ , normal to the flow.  $Q$  is thus related to the dimensionless hydraulic gradient  $i$ , in the direction of the flow and to the hydraulic conductivity  $K$ . The latter is a material property of both the fluid and the geological medium and may be written as

$$K = \frac{k\rho g}{\mu}, \quad (3)$$

where  $k$  is the intrinsic permeability,  $g$  is the acceleration due to gravity ( $9.81 \text{ m/s}^2$ ),  $\mu$  is the dynamic viscosity of the fluid ( $1 \times 10^{-3} \text{ N s/m}^2$  for pure water at  $20^\circ\text{C}$ ) and  $\rho$  is the fluid density ( $998 \text{ kg/m}^3$  for pure water at  $20^\circ\text{C}$ ).

For fluid flow through rock joints, it is common to consider the joint as composed of two smooth parallel plates and the flow to be steady, single phase, laminar and incompressible. Under these conditions, the hydraulic joint conductivity ( $K_j$ ) may be written (after Poiseuille):

$$K_j = \frac{\rho g}{\mu} \frac{e^2}{12} \quad (4)$$

or

$$K_j = \frac{ge^2}{12\nu}, \quad (5)$$

where  $\nu$  is the kinematic viscosity of the fluid ( $1.0 \times 10^{-6} \text{ m}^2/\text{s}$  for pure water at  $20^\circ\text{C}$ ) and  $e$  is the hydraulic aperture. The hydraulic joint conductivity is a parameter expressing the flow through the joint under the influence of frictional losses, tortuosity and channeling; these factors depend on the geometry of the flow channels and the fluid viscosity. Assuming that Darcy's law ( $Q = KiA$ ) can also be applied to flow in rock joints, setting  $A = ew$ , we obtain

$$Q = \frac{g}{\nu} \frac{we^3}{12} i, \quad (6)$$

where  $i$  is the dimensionless hydraulic gradient and  $w$  is the breadth of the flowing zone between the parallel plates. This equation is usually called the "cubic law". One must keep in mind that Eq. (6) is derived for an "open" channel, i.e. the planar surfaces remain parallel and are thus not in contact at any point.

When Darcy's law is applied to natural rock joints with rough surfaces, many researchers [1–3,18] suggests that a correction factor has to be used, which accounts for deviations from the ideal conditions assumed in the parallel smooth plate theory. A study by Zimmerman and Bodvarsson [19] concluded, that the hydraulic aperture is less than the mechanical aperture by a factor that depends on the ratio of the mean value of the aperture to its standard deviation. Results by Hakami [8] showed that the ratio between mechanical mean aperture ( $E$ ) and hydraulic aperture ( $e$ ) was 1.1–1.7 for joints with a mean aperture of 100–500  $\mu\text{m}$ .

On the basis of experimental data (Fig. 3), Barton [14] proposed the following exponential function, relating the hydraulic aperture ( $e$ ) to the mechanical aperture ( $E$ ) and JRC:

$$e = \frac{E^2}{\text{JRC}^{2.5}} \quad (7)$$

One should note that this equation is only valid for  $E \geq e$ . The background data mainly comes from normal deformation fluid flow tests. Just a few cases come from shear deformation fluid flow tests (made on large blocks, [12]). As one can see in Fig. 3, there is a clear trend following an exponential function. The curves illustrated in Fig. 4, show the predicted relation between ( $E/e$ ) and hydraulic aperture ( $e$ ) for different values of JRC, according to Eq. (7).

The JRC coefficient describes the peak roughness of correlated, mated surfaces, and can be estimated either by correctly designed tilt, push or pull tests on jointed rock samples or by visual comparison of measured roughness profiles from the joint surface with a standard set of profiles [21]. The latter is obviously slightly objective, and therefore only an approximate method.

During shearing, this regular exponential behaviour appears to break down. Under an increasing shear

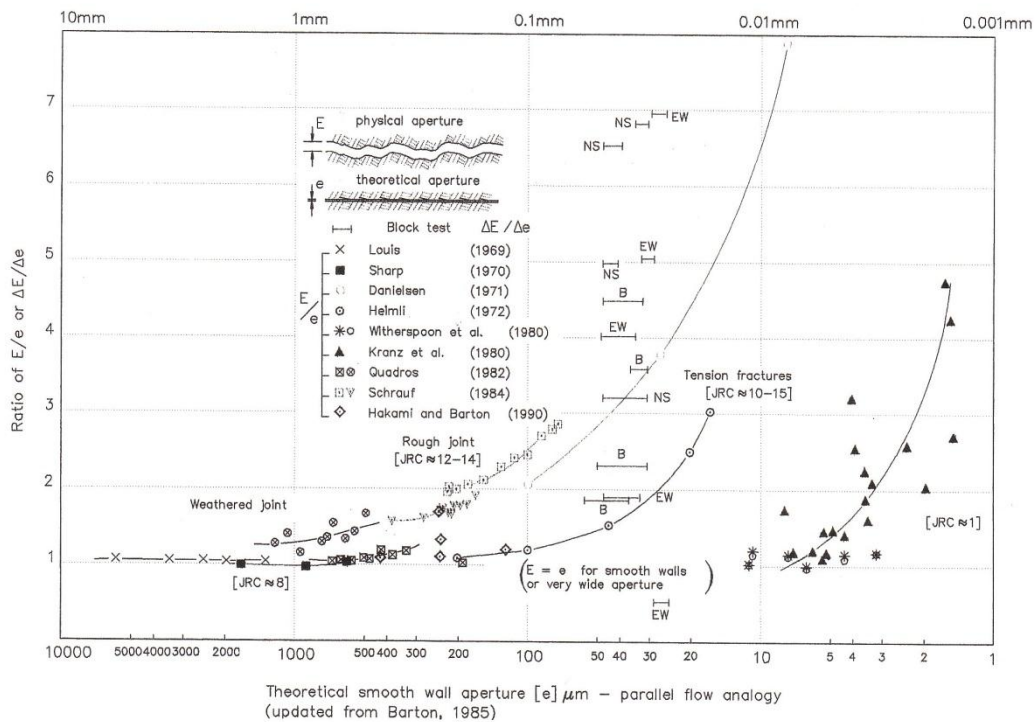


Fig. 3. Comparison of real mechanical apertures ( $E$ ) with theoretical smooth wall conducting apertures ( $e$ ). The mismatch is caused by flow losses due to tortuosity and surface roughness. After Barton [14], with updating by Barton and Quadros [20]. The references listed in this figure are given in full by Barton and Quadros [20].

displacement the joint dilates and both the hydraulic and the mechanical aperture increase. The  $2 \times 2 \times 2$  m in situ block test reported by Hardin et al. [13] gave  $E/e$  ratios that climbed to higher ratios than those given in Fig. 4 when shearing was occurring. The relevant points are plotted as “ $E-W$ ” and “ $N-S$ ” (principal flatjack loads) in Fig. 3. Both the ratio ( $E/e$ ) and the hydraulic aperture may increase in such cases. Therefore, the lines should increase upward to the left in the model in Fig. 4. Such behaviour was also shown by Esaki et al. [22] and most recently by Olsson [16], and is therefore the subject of the suggested improvements.

### 3. Recently performed hydromechanical shear tests

Some results from a major investigation [16,17], concerning the mechanical and hydromechanical behaviour of hard rock joints are presented here and are subsequently used to suggest a modification to the existing model. The present investigation also represented different boundary conditions in the rock

mass, i.e. constant normal stress and constant normal stiffness.

#### 3.1. Sample preparation

The selected tests were performed on granite joints samples, cored in a niche at the side at the access tunnel at the Äspö Hard Rock Laboratory (HRL) in Sweden. This is an underground research laboratory for studying problems related to storage of high-level radioactive nuclear waste. The intact rock had mechanical properties as shown in Table 1.

The cores were drilled parallel to a joint plane. In order to obtain relatively undisturbed samples, two hose clips were applied around each drilled core when the inner end was still fixed in the rock mass. Thereafter, the cores were broken at the inner end and taken out from the rock mass. In order to keep the nominal contact area constant during shearing the cores were cut to a length of around 220 mm and the upper part additionally cut 30 mm, i.e. to a length of around 190 mm. After cutting the samples, two 12 mm holes

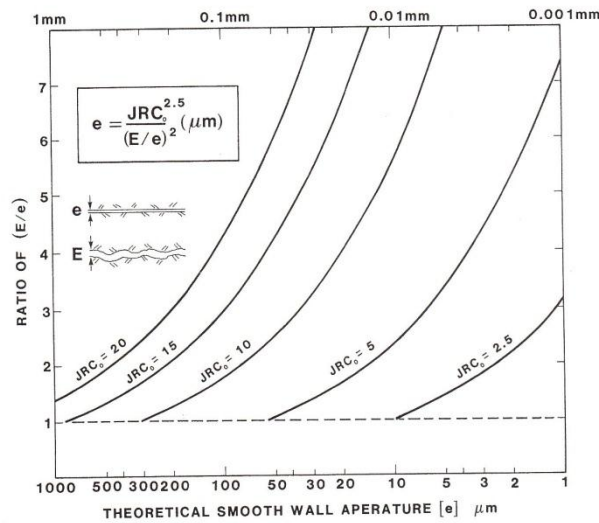


Fig. 4. An empirical relation incorporating joint roughness (JRC) and aperture which broadly satisfies the trends exhibited by available flow data. After Barton [14].

Table 1  
Mechanical properties for the granite

Uniaxial compressive strength $\sigma_c$	169 ± 5 MPa
Young's modulus $E$	59 ± 3 GPa
Poisson's ratio $\nu$	0.25
Tensile strength $\sigma_t$	13.6 ± 2 MPa
Density $\rho$	2760 kg/m <sup>3</sup>

were cored at each end of the lower specimen, two for inlet and two for outlet of water. In the holes, 10 mm copper pipes were then placed, and the two specimen parts were cast into larger concrete blocks to fit in the shear box holders.

The joint roughness, via the JRC, was determined from back-calculation of the shear tests, while the basic friction angle was estimated from shear tests performed on samples with saw-cut, dry surfaces. Tests performed with a Schmidt hammer showed that the JCS value could be set equal to the uniaxial compressive strength. The initial test parameters and joint properties are shown in Table 2.

After preparation and characterisation of the samples, hydromechanical direct shear tests were performed in the shear equipment at Luleå University of Technology, Sweden.

### 3.2. Experimental equipment

The direct shear experiments were performed with servo-hydraulic equipment. In principle, the equipment

Table 2  
Initial test parameters and joint properties

Sample	NT3	N13a	N13c	N14b
$\sigma_{init}$ (MPa)	2	2	2	4
krm (kN/mm)	0	37	75	37
JRC	9.7	7.2	8.8	12.2
$\phi_b$ (deg)	31	31	31	31

is a shear box inside a very stiff steel frame (see Fig. 5). The normal and shear loads were applied by one, respectively, two hydraulic actuators equipped with servo-valves. The normal load is transferred via a spherical and a hydrostatic bearing. This insures that the upper sample holder can move during shearing, with a minimum of friction and bending movement.

A principal illustration of the water flow arrangements is shown in Fig. 6.

Constant water pressure head was obtained by pumping water to the upper vessel (3). The upper vessel was connected to the water inlet of the lower half of the specimen. Mostly, the water had been stored for around 1–2 days in an open container (1). After passing the joint, the water was weighed (5) for calculation of the water flow rate. The weight was recorded every second by use of two load cells (6).

### 3.3. Experimental procedures

Before the shear tests, two and a half normal loading-unloading cycles were performed to consolidate the

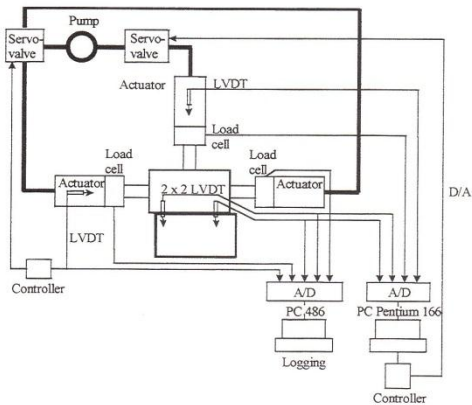


Fig. 5. Schematic block diagram for the shear control system.

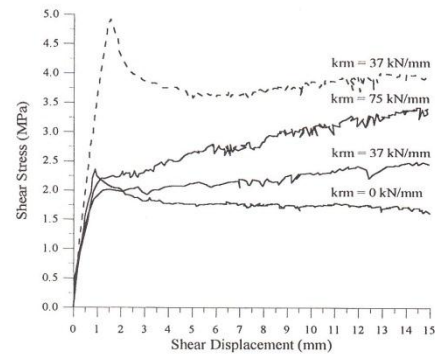


Fig. 7. Shear stress versus shear displacement for four shear tests with different rock mass stiffnesses ( $k_{rm} = 0, 37$  and  $75$  kN/mm) and initial normal stresses. The three tests with solid lines had an initial normal stress of 2 MPa, and the test with dashed lines had an initial stress of 4 MPa.

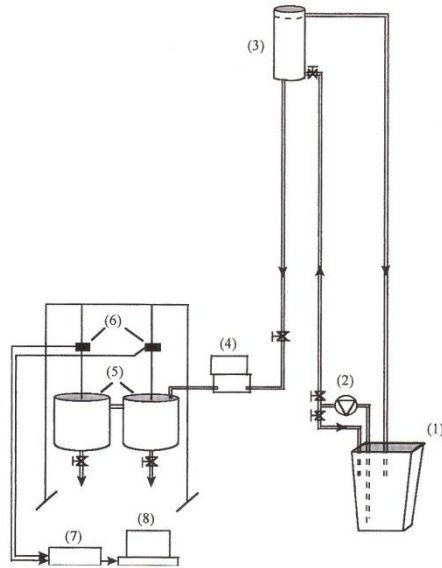


Fig. 6. Principle illustration of the set-up for hydromechanical direct shear tests. (1) Stored water, (2) pump, (3) upper vessel, (4) joint specimen with an all-round rubber seal, (5) vessels for measuring of used water, (6) load cells, (7) A/D transducer and (8) 486 PC.

joints. The maximum load was the same as later used for the shear tests.

The shear tests were performed at two normal stresses ( $\sigma_n = 2$  and 4 MPa) and with three loading conditions: constant normal load (CNL) where the rock mass stiffness  $k_{rm} = 0$ , and constant normal stiffness (CNS) where the rock mass stiffness  $k_{rm}$  was either 37 or 75 kN/mm. In the CNL tests, the joint was allowed to dilate

with no increase of the normal load, while during the CNS tests, a hydraulic spring load provided constant normal stiffness [16]. The load was linearly proportional to the normal displacement and was measured by four gauges at a given constant normal stiffness. After a total shear movement of around 15 mm, the shear movement was stopped and the normal load removed.

At the “upstream” end of the joints, a water pressure head of 4 m was applied. After passing the inlet pipes, the water were evenly distributed over the whole width of the joint. At the “downstream” end of the joints the water was collected and weighed for flow rate estimation.

### 3.4. Experimental results and analysis

#### 3.4.1. Shear stress

As can be seen in Fig. 7, there is a deviation in the shear stress accumulation after passing the peak value between CNL and CNS shear tests. As usual during CNL tests, there is first a quick rise in the shear stress up to a maximum peak value ( $\tau_p$ ), followed by a gradual decline to a residual value ( $\tau_r$ ). But for CNS tests after passing the quick rise, there is an increase of the shear stress, instead of a slow decrease, until a constant value is obtained after a large shear displacement. This is due to the increasing normal stress from the rock mass stiffness. As one also can see in the figure, as the normal stress and stiffness increases the shear stresses also are augmented.

#### 3.4.2. Normal behaviour

The corresponding normal displacement (volume change) versus shear displacement is shown in Fig. 8. During a short initial shearing, the normal displacement is in a state of slight contraction, which is followed by

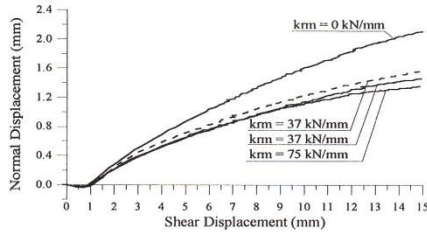


Fig. 8. Normal displacement versus shear displacement for four shear tests showed in Fig. 7.

dilation. The maximum normal displacement occurs as the shear stress attains a residual value, but the maximum rate of dilation corresponds to the preliminary peak shear strength. Due to the increasing normal stress during CNS tests, the dilation is less for CNS than for CNL.

3.4.3. Stress paths during shearing

Concerning the stress paths shown in Fig. 9, the CNL and CNS tests exhibit differences.

In each case, the shear stress rises to a preliminary peak. In the CNS tests, the shear stress then slowly rises further while in the CNL test it falls to a preliminary residual value of shear stress. The maximum value is commonly used for estimation of a shear strength curve. In Fig. 9, the peak shear strength value for CNL test is marked with a triangle.

Peak shear strength curves were calculated according to

$$\tau_p = \sigma_n \tan \left[ \text{JRC} \log_{10} \left( \frac{\text{JCS}}{\sigma_n} \right) + \phi_r \right], \quad (8)$$

where  $\sigma_n$  is the normal stress, and  $\phi_r$  is the residual friction angle. These are shown as fine dotted curves in Fig. 9. To generate these curves, it has been assumed that  $\text{JCS} = \sigma_c = 215 \text{ MPa}$  and  $\phi_r = \phi_{b0} = 32^\circ$ . Four different values of JRC have been used. These envelopes correspond best with the peak value for the CNL test but also quite well for the CNS tests.

3.4.4. Hydromechanical behaviour

The most evident hydromechanical coupling during the shear tests is between the shear displacement and the transmissivity ( $T$ ). The transmissivity is defined as

$$T = \frac{Q}{wi} \quad (9)$$

The transmissivity is seen to increase at least an order of magnitude with 4 or 5 mm of shearing in all the cases studied. As one can see in Fig. 10, the transmissivity decreased with higher rock mass stiffness and initial normal stress because joints suffer a normal stress increase under CNS tests.

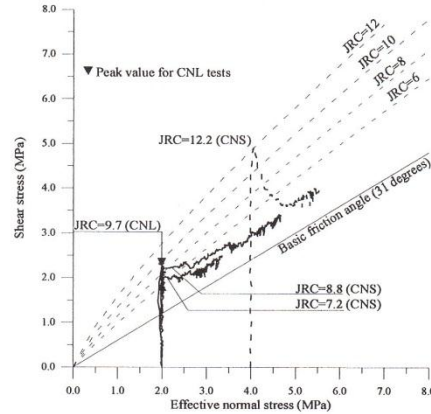


Fig. 9. Shear stress versus effective normal stress for four shear tests showed in Fig. 7.

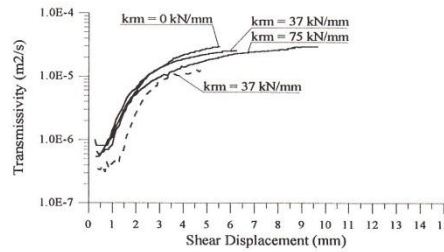


Fig. 10. Transmissivity versus shear displacement for the four shear tests shown in Fig. 7.

3.4.5. Mechanical and hydraulic aperture

In order to plot the changes of the mechanical aperture versus the hydraulic aperture during shear deformation (Fig. 11), we first assumed that the changes of the mechanical aperture are equal to the dilation of the rock joint. The mechanical aperture ( $E = E_0 + \Delta E$ ) was calculated by adding the changes of dilation ( $\Delta E$ ) to an initial aperture ( $E_0$ ) equal to the mechanical aperture at the end of the normal loading cycles. No real initial mechanical aperture were measured, only closure/opening of the joints. As the initial mechanical aperture not was measured before the shear tests, the final hydraulic aperture from the loading/unloading tests was used for estimations using Eq. (7). Thereafter, ratios of  $E/e$  were calculated for each 0.5 mm interval and plotted versus  $e$  in Fig. 12.

In Fig. 11, the mechanical aperture and the hydraulic aperture versus shear displacement are plotted for the four tests. As one can see in the figure, the increase in mechanical aperture is greater than that of the hydraulic aperture after passing the peak shear stress (obtained at around 1–2 mm shear displacement).

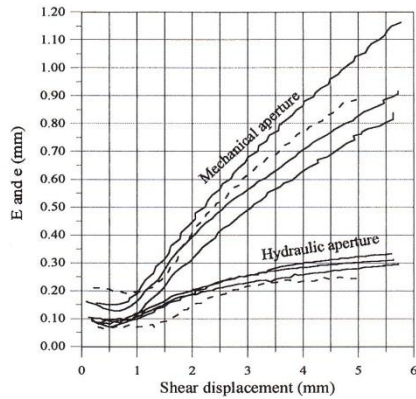


Fig. 11. Measured joint closure and calculated hydraulic aperture versus shear displacement for hydromechanical direct shear tests.

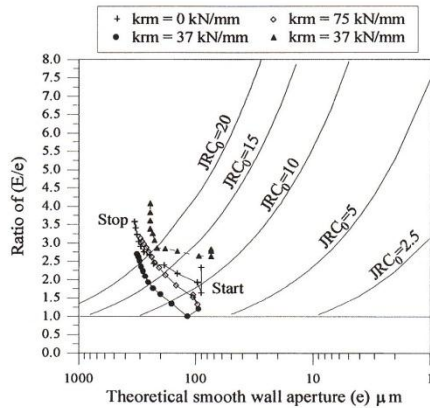


Fig. 12. Calculated  $E/e$  versus  $e$  for the tests in Fig. 4 in a diagram suggested by Barton [14]. Breakdown is indicated, due to the shearing.

For predictions of fluid flow in hydraulic models the hydraulic aperture is obviously used. However, during numerical modelling of rock mass deformation, using for example the distinct element UDEC code [23], the joint opening or closing is first calculated. When shearing does not occur, conversion between mechanical aperture and hydraulic aperture can follow the trends shown in Figs. 3 and 4. However, when shearing and dilation occur, the interlocking asperity geometry begins to breakdown.

As one can see in the Fig. 12,  $E/e$  increases in a reversed manner, compared to the other curves in the figure. This was expected, following the results in Fig. 11; however, it is contrary to what was suggested in the original model [14], which was mostly based on normal closure-flow coupling data (see Fig. 3). Such a

deviation, was also shown by Esaki et al. [22] and by Barton [14] as mentioned earlier. However, a good explanation was not developed.

In the case of Esaki et al. [22] tests, the joints in sandstone were loaded to more than 50% of the uniaxial compression strength. Production of gouge probably caused the high  $E/e$  ratios (maximum  $E/e=25$ ). Gouge production also caused some CSFT (coupled shear-flow tests) reported by Makurat et al. [24] to show reduced permeability in relation to the predicted (maximum) effect of dilation. The original  $E/e$  versus JRC model [14] is in fact almost exclusively based on normal compression or opening tests and comparisons between true (measured) mechanical apertures and hydraulic apertures. During increased normal stress, the hydraulic aperture ( $e$ ) decreases, which causes an increase in  $E/e$  due to tortuosity. This behaviour tends to follow the “ $JRC_0$  curves” in Fig. 4.

During the first part of each plotted shear path in Fig. 12, the  $E/e$  ratio is first slightly decreasing and thereafter increasing. This initial part belongs to the pre-peak and peak shear displacement when the asperities along the joint walls are not destroyed and the hydraulic aperture is probably decreasing due to shear-related closing of small voids. Thereafter, the geometry of the joint walls is in a changing phase, (the so-called “breakdown”) where the asperities get worn and damaged under the increasing shear deformation. The size of roughness degradation (decrease in mobilized JRC) depends on the strength of the asperities, on the applied normal load and on the shear deformation. Furthermore, new flow paths open and others close due to the increasing areas of contact between the joint walls and due to gouge production. For this behaviour, a conceptual model visualising reduction of joint porosity with increasing gouge production has been suggested [20]. The gouge production will probably decrease the hydraulic aperture. So, the increase in  $E/e$  during shearing depends not on the same phenomena as during normal loading and unloading. In the recent literature, some reported tests [25,26] have shown that after passing the peak displacement, the principal flow paths may reorient and become directed nearly perpendicular to the shear direction. This is not incorporated in the model at present, as it may not be a general result. Conceptually, it is difficult to imagine elongated areas of wear allowing greater perpendicular flow. However, if the elongations of constant areas are oriented perpendicular to the shear direction, such could be readily understood.

#### 4. A model for hydromechanical coupling during shearing of rock joints

An improved model is therefore proposed on the basis of the performed hydromechanical shear tests [11] and

based on the above discussion. It is an empirical engineering model and not a theoretical scientific model and is built on the  $E/e$  versus  $e$  curves for the four tests reviewed before. Further, it is not a reversible model. As shear tests on rough rock joints are composed of at least two major parts, pre-peak/peak and post-peak, the model considers these two basic phases. For the first phase, the coupling between the mechanical and hydraulic aperture assumes more or less interlocked, matched joint walls. This starting value of the hydraulic aperture is the final value from the normal loading cycle and can be calculated by Eq. (7):

$$e = \frac{JRC_0^{2.5}}{(E/e)^2}$$

This “starting point” applies also to shear displacement ( $u_s \leq 0.75u_{sp}$  (peak shear displacement)).

The second phase for  $u_s \geq u_{sp}$  can be calculated by

$$e = \left(\frac{E}{e}\right) JRC_{mob}^2 \quad (10)$$

Eq. (10) applies to values of  $JRC_{mob} > 0$ , i.e. joints with finite roughness ( $JRC_0 > 0$ ) and with a residual roughness despite shearing. In the first phase, where the joint wall roughness is not destroyed, the peak  $JRC_0$  should be used. In the second phase, where the geometry of the joint walls is changing with increasing shear displacement, the  $JRC_{mob}$  (mobilized value of JRC) should be used [14]. During this phase, gouge is being produced but as the joint is dilating some of the gouge is probably flushed to the sides of developing flow channels. The value of  $JRC_{mob}$  is dependent on the strength on the joint surface (JCS), on the applied normal stress ( $\sigma_n$ ) and on the magnitude of the shear displacement. It is also dependent on the size of joint plane ( $L_n$ ) and on the residual friction angle ( $\phi_r$ ). The intermediate phase, between phase one and two ( $u_s = 0.75u_{sp}$  to  $u_{sp}$ ), is difficult to define with any model and it is recommended for the present that the two phases are connected with each other by a transition curve.

For the calculations of  $JRC_{mob}$  the following relevant data were used:  $JCS = \sigma_c = 169$  MPa,  $\sigma_n = 2$  MPa and  $\phi_r = \phi_b = 31^\circ$ . For the illustration of the model, an example is shown in Fig. 13. As one can see in the figure, the curves have a break (●), which is the boundary where Eq. (10) starts to apply, i.e. at the peak shear strength. The position of the start points (0) for shearing depends on the assumed initial mechanical aperture ( $E_0$ ). A lower start value for  $E_0$  moves the starting point up to the right along the initial part of each  $JRC_0$  curve and vice versa (e.g. Figs. 3 and 4).

If the curves in Fig. 13 are plotted in Fig. 4, a more comprehensive figure is obtained, as shown in Fig. 14. The dashed lines belong to the original model in Fig. 4.

As one can see in Fig. 14, the curves for shear behaviour are more vertical than they were for normal

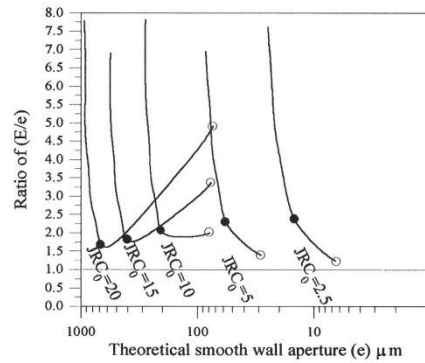


Fig. 13. A plotted example for the empirical relations proposed by Eqs. (5) and (6) incorporating JRC and joint aperture which broadly satisfies the trends exhibited from the tests shown in Fig. 5.

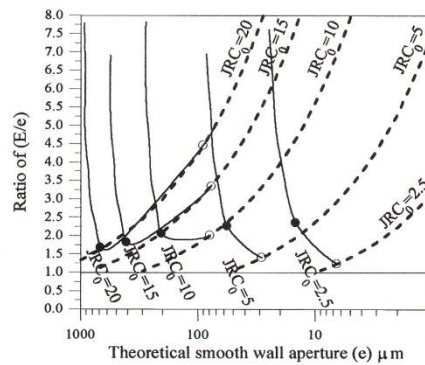


Fig. 14. Curves relating the hydraulic aperture  $e$  and the ratio  $E/e$  for both normal loading/unloading and shear behaviour (with parameters mentioned above and extended curves to fit the entire plot).

loading/unloading behaviour. This is also in agreement with the coupled shear-flow results from Esaki et al. [22] and block test shear-flow results given by Barton [14].

### 5. Comparison between modelled and measured hydraulic conductivity during shearing of rock joints

In order to compare the results from the improved model, composed of Eqs. (7) and (10), with the original model, composed only of Eq. (7), an example is shown below. After determining the JRC coefficient and assuming the initial mechanical aperture before shearing one has to calculate the changes of the mechanical aperture and variation of  $JRC_{mob}$  with shearing.

For the mechanical behaviour, a dimensionless model [14] for CNL shear tests is used (see Fig. 15). In the model, the shear resistance of a joint is calculated, using the concept of mobilised friction, which is a function of JRC, JCS,  $\phi_r$  and  $L_n$  (length of joint). The key aspects, concerning the modelling of the joint behaviour, are described as follows (in the order they occur during a shear event) [14]:

- Friction is mobilised immediately upon initiation of shearing.
- Dilation begins when the roughness is mobilised (assumed at  $u_s/u_{sp} = 0.3$ ).
- Peak strength is reached at  $JRC_{mob}/JRC_p = 1.0$ .
- Dilation declines as the roughness reduces ( $u_s > u_{sp}$ ).
- Residual strength is finally reached after a large shear displacement (e.g.  $u_s \approx 100u_{sp}$ ).

The peak shear displacement ( $u_{sp}$ ) was estimated from

$$u_{sp} = \frac{L_n}{500} \left( \frac{JCS_n}{L_0} \right)^{0.33}, \quad (11)$$

where  $L_0$  is the laboratory-scale joint sample length and  $L_n$  is the field-scale length (i.e. the spacing of cross-joints that gives the effective block size). In this modelling attempt,  $L_n$  was set equal to  $L_0$ .

The mobilised friction angle can be calculated by the following equation for each of the above-mentioned stages:

$$\phi_{mob} = JRC_{mob} \log_{10}(JCS/\sigma_n) + \phi_r \quad (12)$$

and the current shear strength for any shear displacement can be obtained from

$$\tau_{mob} = \sigma_n \tan[(JRC_{mob} \log_{10}(JCS/\sigma_n) + \phi_r)]. \quad (13)$$

The dilation curve ( $u_n$  versus  $u_s$ ) can be calculated by the following expression:

$$\Delta u_n = \Delta u_s \tan d_{nmob}, \quad (14)$$

$$d_{nmob} = \frac{1}{M} JRC_{mob} \log_{10}(JCS/\sigma_n), \quad (15)$$

where  $d_{nmob}$  is the mobilised dilation angle and  $M$  is a damage coefficient, given values of 1 or 2 for shearing under low or high normal stress, respectively.

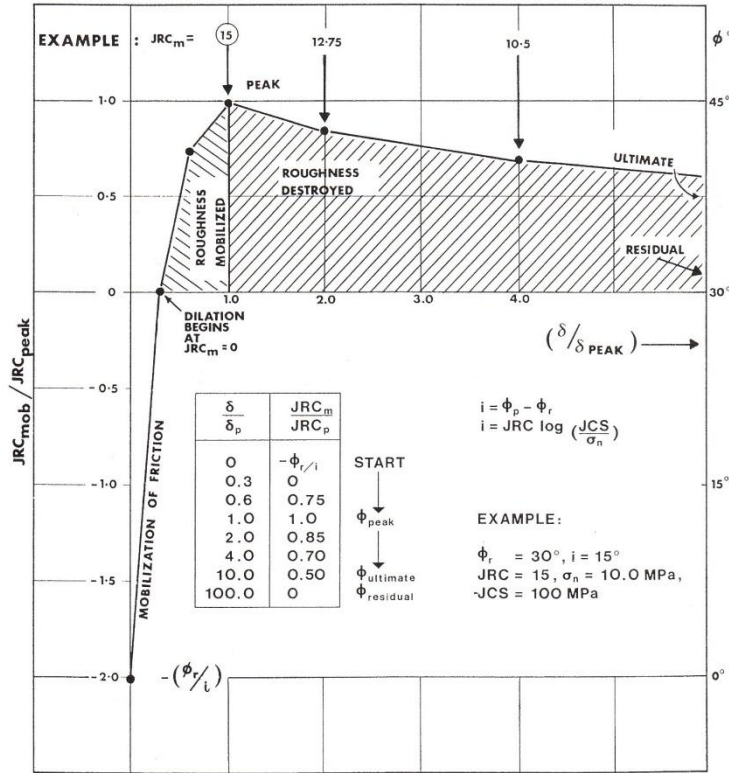


Fig. 15. Recommended dimensionless model for generating realistic shear stress versus shear displacement ( $\delta = u_s$ ) plots for non-planar joints [14].

For initial values of  $JRC_{mob}/JRC_p$ , the ratio  $-\phi_r/i$  is used, where [14]

$$i = JRC \log_{10}(JCS/\sigma_n). \quad (16)$$

Thereafter, the values of  $JRC_{mob}/JRC_p$  in the table in Fig. 15 should be used.

The hydraulic conductivity was calculated according to

$$K = \frac{ge^2}{12\nu}, \quad (17)$$

where the hydraulic aperture was determined by Eq. (7) and by rewriting Eq. (10):

$$e = \frac{E^2}{JRC_0^{2.5}}, \quad u_s \leq 0.75u_{sp},$$

$$e = \sqrt{E} JRC_{mob}, \quad u_s \geq u_{sp}.$$

The mechanical aperture was calculated as

$$E = E_0 + \Delta E, \quad (18)$$

where  $\Delta E$  (caused by joint dilation) can be taken as the tangent of the dilation angle (Eq. 14). A given increment of shear displacement will result in a positive  $\Delta E$  component:

$$\Delta E = \Delta u_s \tan d_{mmob}. \quad (19)$$

By combining Eqs. (14) and (18) one can calculate the mechanical aperture:

$$E = E_0 + \Delta u_s \tan \left[ \frac{1}{M} JRC_{mob} \log_{10}(JCS/\sigma_n) \right]. \quad (20)$$

Usually, the mechanical aperture ( $E_0$ ) is the initial aperture when shearing starts.

For comparison, only one of the hydromechanical shear tests was modelled. This test was a CNL test. The rest of the tests were CNS tests, which the model is not developed for, unless as part of the UDEC-BB version of UDEC, where stress change during shearing is automatically modelled. The following data was used for the modelling:

$$JRC = 9.7,$$

$$JCS = 169 \text{ MPa} (= \sigma_c),$$

$$\phi_r = 31^\circ (= \phi_b).$$

The sample had a length of 0.2 m and was affected by a normal stress of 2 MPa.

As one can see in Fig. 16, both predicted shear stress and the dilation follows the test results quite well. For the hydraulic conductivity, the curve that is predicted by Eqs. (7) and (10) agrees best with the test result, which confirms the potential promise of the new model. The hydraulic conductivity predicted by only Eq. (7) is too high compared to the test results. This confirms that this equation should be used for normal closure/opening tests and only during the start of a shear test, where

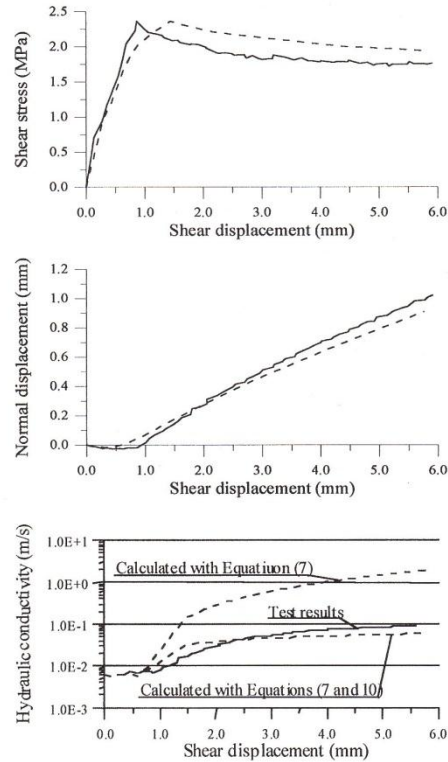


Fig. 16. Shear displacement versus shear stress, normal displacement and hydraulic conductivity for predicted and performed CNL shear test (solid line (—) is performed and dashed line (---) is predicted).

the influence of roughness on flow losses is effectively stronger than when dilation is occurring and where limited damage or gouge production occurs. It can also be noted in Eq. (10) that a rapidly reducing  $JRC_{mob}$  value due to post-peak asperity damage will have the desired effect of reducing the hydraulic aperture.

## 6. Conclusions

(1) Hydromechanical shear tests have shown that a widely used constitutive model [14,15], also included in the UDEC-BB code, yields results that are most suitable for normal loading and unloading and for shear with limited damage or gouge production.

(2) Coupled shear-flow test results show that both the ratio  $E/e$  and the hydraulic aperture ( $e$ ) increase during increased shear displacement.

(3) In this paper, an improved empirical engineering model is proposed for coupling between the mechanical

and hydraulic aperture including the joint roughness coefficient (JRC) for predictions of fluid flow through rock joints. The model consists of two parts which are dependent on the shear displacement:

$$e = \frac{E^2}{\text{JRC}_0^{2.5}}, \quad u_s \leq 0.75u_{sp},$$

$$e = E^{1/2} \text{JRC}_{\text{mob}}, \quad u_s \geq u_{sp}.$$

(4) A first modelling attempt has shown a promising, improved agreement between the predicted and measured hydraulic conductivity for a hydromechanical shear test performed on a granite joint sample. Despite the fact that the model is proposed based on hydro-mechanical shear tests on granite rock joints, we also recommend its use on other rock types but with due caution.

(5) For engineering modelling of conductivity changes of rock joints during shearing, one has therefore first to assume the initial JRC value and the initial mechanical aperture. Thereafter, one has to calculate the changes of the mechanical aperture and  $\text{JRC}_{\text{mob}}$  during shearing. This can be done with a dimensionless model for shear behaviour. These parameters should then be used in Eqs. (7) and (10) to calculate the changes of the hydraulic aperture during shearing. Thereafter, it is possible to calculate either the hydraulic conductivity or transmissivity.

(6) Further work will be needed in order to incorporate the improved model in the UDEC code.

#### Acknowledgements

The first author would like to thank the Swedish Nuclear Fuel and Waste Management Company (SKB) for the financial support during the experimental phase, and also Grøner AS for support during writing of this paper. The second author would like to thank nuclear waste research funding by ONWI and AECL of the USA and Canada, who supported our rock mechanics developments in the 1980s. Colleagues Bandis and Bakhtar made special contributions.

#### References

- [1] Witherspoon PA, Wang JSY, Iwai K, Gale JE. Validity of cubic law for a deferrable rock fracture. *Water Resources Res*, 1980;16(6):1016–24.
- [2] Elliot GM, Brown ET, Boodt PI, Hudson JA. Hydromechanical behaviour of the Carnmenellis granite, S.W. England. In: Stephansson O, editor. *Conference Proceedings, International Symposium on Fundamentals of Rock Joints*, Sweden: Björkliden, 1985. p. 249–58.
- [3] Zhao J, Brown ET. Hydro-thermo-mechanical properties of joints in the Carnmenellis granite. *Quart J Engng Geol* 1992;25:279–90.
- [4] Larsson E. Groundwater flow through a natural fracture — flow experiments and numerical modelling. Licentiate Thesis, Department of Geology, Chalmers University of Technology, Gothenburg, Sweden, Publ. A 82, 1997.
- [5] Pine RJ. Rock joint and rock mass behaviour during pressurised hydraulic injection. Ph.D. Thesis, Camborne School of Mines, Cornwall, UK, 1986.
- [6] Rutqvist J. Coupled stress-flow properties of rock joints from hydraulic field testing. Ph.D. Thesis, Division of Engineering Geology, Royal Institute of Technology, Stockholm, 1995.
- [7] Bandis SC. Engineering properties and characterization of rock discontinuities. In: *Comprehensive Rock Engineering. Principles, Practice & Projects*, vol. 1: Fundamentals, 1993. p. 155–18.
- [8] Hakami E. Aperture distribution of rock fractures. Ph.D. Thesis, Division of Engineering Geology, Royal Institute of Technology, Stockholm, 1995.
- [9] Sharp JC, Brawner CO. Prediction of the drainage properties of rock masses. Theme 4, International Symposium on Percolation through Fissured Rock, Stuttgart, 1972.
- [10] Sharp JC, Maini YNT. Fundamental considerations on the hydraulic characteristics of joints in Rock. Paper T1-F, International Symposium on Percolation through Fissured Rock, Stuttgart, 1972.
- [11] Barton N. The problem of joint shearing in coupled stress-flow analyses. Discussion D4, International Symposium on Percolation through Fissured Rock. Stuttgart, 1972.
- [12] Makurat A. The effect of shear displacement on the permeability of natural rough joints. *Hydrogeology of rocks of low permeability*. Proceedings of the 17th International Congress on Hydrogeology, Tucson, Arizona, USA, 1985. p. 99–106.
- [13] Hardin EL, Barton N, Lingle R, Board MP, Voegele MD. A heated flatjack test series to measure the thermomechanical and transport properties of in situ rock masses. Office of Nuclear Waste Isolation, Columbus, Ohio, ONWI-260, 1982. 193pp.
- [14] Barton N. Modelling rock joint behaviour from in situ block tests: implications for nuclear waste repository design. Office of Nuclear Waste Isolation, Columbus, OH, ONWI-308, 1982. 96pp.
- [15] Barton N, Bandis S, Bakhtar K. Strength, deformation and conductivity coupling of rock joints. *Int J Rock Mech Min Sci Geomech Abstr* 1985;22:121–40.
- [16] Olsson R. Mechanical and hydromechanical behaviour of hard rock joints — a laboratory study. Ph.D. thesis, Chalmers University of Technology, Gothenburg, Sweden, 1998. p. 197.
- [17] Olsson R. Mechanical and hydromechanical behaviour of hard rock joints — a laboratory study. Addendum, Report 1999:6, Chalmers University of Technology, Gothenburg, Sweden, 1999. p. 34.
- [18] Zhao J. Effect of normal stress and temperature on hydraulic properties of rock fractures. Conference Proceedings on Memories of the XXIV Congress of IAH, Oslo, Norway, 1993. p. 115–22.
- [19] Zimmerman RW, Bodvarsson GS. Hydraulic conductivity of rock fractures. *Transport Porous Media* 1996;23:1–30.
- [20] Barton N, Quadros EF. Joint aperture and roughness in the prediction of flow and groutability of rock masses. *Int J Rock Mech Min Sci*, 1997;34(3–4), Paper No. 252.
- [21] Barton N, Choubey V. The shear strength of rock joints in theory and practice. *Rock Mech* 1977;10:1–54.
- [22] Esaki T, Ikusada K, Aikawa A, Kimura T. Surface roughness and hydraulic properties of sheared rock. *Fractured and Jointed Rock Masses*, Lake Tahoe, CA, 1995. p. 93–8.
- [23] Cundall PA. A generalized distinct element program for modelling jointed rock. Report PCAR-1-80. Contract DAJA37-79-C-0548, European Research Office, US Army, Peter Cundall Associates, 1980.

- [24] Makurat A, Barton N, Rad NS, Bandis S. Joint conductivity variation due to normal and shear deformation. Proceedings of the International Symposium on Rock Joints, Balkema, Loen, Norway, 1990. p. 535–40.
- [25] Gentier S, Lamontagne E, Archambault G, Riss J. Anisotropy of flow in a fracture undergoing shear and its relationship to the direction of shearing and injection pressure. *Int J Rock Mech Min Sci* 1997;34(3–4), Paper No. 094.
- [26] Gentier S, Riss J, Hopkins D, Lamontagne E. Hydromechanical behaviour of a fracture: how to understand the flow paths. Proceedings of the Third International Conference on Mechanics of Jointed and Faulted Rock, Vienna, Austria, 1998. p. 405–22.